Available online at www.sciencedirect.com
ScienceDirect
Journal of Power Sources 171 (2007) 294–301
JOURNAL OF POWER SOURCES
www.elsevier.com/locate/jpowsour

Enhancing PEM fuel cell performance by introducing additional thin layers to sputter-deposited Pt catalysts

D. Gruber *, J. Müller

Department of Micro Systems Technology, Hamburg University of Technology, D-21071 Hamburg, Germany

Received 2 August 2006; received in revised form 20 June 2007; accepted 23 June 2007
Available online 1 July 2007

Abstract

Polymer electrolyte membrane (PEM) fuel cells with sputter-deposited Pt catalyst thin films and different sublayers added before the deposition of the Pt films to enhance the fuel cell performance are presented. Comparison of the performance of the fuel cells shows, for example, that thin films of Cr or silicone-like layers enhance the performance of the prepared cells of 15 mm × 15 mm electrode area. The achieved peak power density at room temperature and ambient pressure for a H_2/O_2 operated fuel cell loaded with 0.054 mg cm^{-2} (25 nm) Pt per electrode was 210 mW cm^{-2}. Addition of a thin layer of Cr (1 nm) underneath the catalyst layer (0.054 mg cm^{-2} Pt) improved the maximum power density to 259 mW cm^{-2}. Scanning electron microscopy analysis showed that this is due to the change in morphology of the growth of the Pt catalyst layer on the Cr seeds.

The performance of fuel cells prepared for reference from commercially catalyzed electrodes with standard carbon-supported Pt loadings of 0.5 and 1 mg cm^{-2} could be improved after treatment of the electrodes in an oxygen plasma. The physically assisted removal of carbon and CF-groups from the surface in the oxygen plasma most likely uncovers more Pt sites from the carbon-supported Pt catalyst.

Keywords: Sputter deposition; Thin film sublayer; Platinum catalyst; Polymer electrolyte membrane (PEM) fuel cell

1. Introduction

For polymer electrolyte membrane (PEM) fuel cells high costs are still associated with the amount of Pt catalyst that is needed. This metal is precious and its supply is limited [1].

Recently many efforts are undertaken to improve the catalyst utilization. Following is a concise list of the most significant efforts that are under investigation to evade this impediment. Besides the development of non-platinum catalysts [2], ways to utilize the Pt catalyst more efficiently by increasing the active area of the catalyst particles or catalytic activity and reduce its loading are investigated. This can, for instance, be accomplished by using and optimizing standard carbon-supported catalysts [3–6] or by sputter deposition of catalyst thin films [7–10]. Recently, Adžić and coworkers presented a new method to reduce the Pt loading by the deposition of Pt submonolayers on Ru nanoparticles [11–13]. The thus prepared electrocatalysts had a higher activity and CO tolerance than commercial catalysts containing serveral times higher Pt loadings. Electronic effects appear to be responsible for this enhancement of Pt submonolayers on Ru [14]. Under real fuel cell operating conditions, Gullá et al. reported of electrodes prepared by a dual ion-beam assisted deposition technique with low Pt loadings of 0.04–0.12 mg cm^{-2} that showed more effective catalyst utilization and enhanced activity than commercial electrodes of significantly higher loadings [15]. Enhanced catalytic activity was also found if Pt was alloyed with various transition metals [16–20]. They are less expensive and can also help to improve the CO tolerance of the catalyst [20–22]. Among the proposed explanations for this activity enhancement are a change in interatomic spacing or electronic effects influencing the electronic states [23–25]. Furthermore, the use of carbon nanotubes, nanocoils, or nanofibers as support for fuel cell catalyst has shown to enhance the catalyst activity [26–31], which can be attributed to a higher catalyst surface area and change in morphology [32].

In this article, an approach of adding thin sublayers underneath the sputter-deposited Pt catalyst is presented. Results for electrodes with sputter-deposited low Pt loadings and the effect

* Corresponding author. Present address: NXP Semiconductors Germany GmbH, Stresemannallee 101, D-22529 Hamburg, Germany.
E-mail address: d.gruber@tuhh.de (D. Gruber).

0378-7753/$ – see front matter © 2007 Elsevier B.V. All rights reserved.
doi:10.1016/j.jpowsour.2007.06.232

on the performance of mixing different layers in the Pt catalyst were presented in a previous work [33]. It showed that sputter deposition can be highly effective as the catalyst material is applied to the electrode directly and the three-phase boundary (electrode–catalyst–PEM) is formed in a series of precise deposition processes avoiding any application of solution or ink containing arbitrarily distributed catalyst material, which may cause the catalyst to be only partly in contact with the proton-conducting membrane or electrode and many catalyst sites to keep passive. The growth of the sputter-deposited Pt thin films was characterized and also first results for fuel cells with added sublayers of Cr and Pd were presented. The results with two 1 nm thin layers of Cr added in the Pt catalyst layer showed improved performance and the analysis of SEM images revealed that a change in morphology of the growing Pt layer is observed. Noticing that the performance increase is associated with the change in morphology rather than a catalytic effect of the Cr (no effect if Cr is added as top layer), one single Cr thin layer is now inserted underneath the catalyst layer, i.e., before the deposition of the Pt instead of the two Cr layers previously mixed in the Pt layer. Thin layers of Pd had equally been added to both, anode and cathode side. The observed increase in performance could not be attributed to any morphological change in layer composition and led to the assumption that it is associated with the hydrogen permeability of the added Pd and the improved hydrogen fuel distribution on the anode side.

In this work the effect of sublayers, which are applied as an incipient or seeding thin layer on a standard uncatalyzed electrode material prior to the sputter deposition of the Pt catalyst, on the performance of the Pt catalyst in fuel cell operation is investigated.

2. Experimental

The fuel cells were prepared from catalyzed and uncatalyzed ELAT electrodes (E-TEK Division, PEMEAS). All the porous electrodes used in the present paper were from the same lot which allows for a true comparison of the subsequent results.

Different amounts of Pt catalyst were applied to the uncatalyzed ELAT electrodes by sputter deposition from a Pt diode target of 150 mm diameter. This was done at a fairly low rf power of 50 W at room temperature and a pressure of 2 Pa to allow an accurate control of the deposited layer thickness and avoid any thermal or mechanical stress on the electrode substrates. The catalyst loading was controlled by the sputter rate and time. Based on the thickness (measured on a solid reference sample rather than the porous electrode substrate) and the density of the material the catalyst loading of the 15 mm × 15 mm electrodes was determined.

Using these electrodes with the sputtered catalyst and Nafion 115 membranes (DuPont), membrane electrode assemblies (MEAs) were fabricated in a hot bonding process at 140 °C and a pressure of 290 kPa using Nafion solution (5%, Sigma–Aldrich). The latter was applied to the Nafion 115 membrane at loadings of $\leq$1.5 mg cm^{-2} and not to the catalyst nanolayers on the porous electrodes to avoid an instant occlusion.

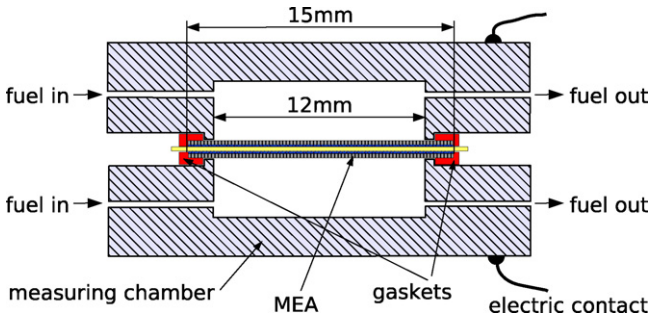

Fig. 1. Schematic cross-sectional view of the used measuring chamber for the characterization of the MEAs.

Throughout this paper the given Pt loadings refer to the loading per electrode. All investigated fuel cells have equal amounts of Pt loading on the anode and cathode side.

For control, reference MEAs were fabricated from catalyzed ELAT electrodes with 0.5 and 1 mg cm^{-2} Pt loading. Additionally the front side of such commercial electrodes were treated in an oxygen plasma process (25 sccm O_2, 50 W, 2.3 Pa) for 3 min before the MEAs were assembled.

The MEAs were characterized in a measuring chamber as depicted in Fig. 1. Two metal plates with cavities of 12 mm × 12 mm supply the fuels to the MEA (active electrode area of 15 mm × 15 mm) placed in between. The part of the MEA exceeding the 12 mm × 12 mm is compressed between the metal plates and gasket to provide good electric contact and seal the cell, even though this may lead to an inefficient direct fuel supply to the active electrode area there.

Hydrogen and oxygen were supplied to the fuel cells by mass flow controllers at 20 and 4 sccm, respectively. All measurements were carried out at room temperature (21 °C) and ambient pressure. To simulate the load of the fuel cell a variable potential was applied to a resistance set in parallel to the fuel cell.

A personal computer controls the load and collects the resulting cell voltage and current density from a set of data acquisition units. For each presented data a minimum of two samples has been prepared and measured.

As additional sublayers Cr, Pd, and silicone-like layers have been deposited underneath the Pt thin film, i.e., between the porous ELAT electrode substrate and the catalyst. Chromium was sputtered from a 150 mm Cr diode target at 50 W rf power, a pressure of 2 Pa and room temperature. Cr and Pt were sputtered in the same vacuum chamber without breaking the vacuum to avoid any oxidation. The Pd thin films were applied by vapor deposition ($\leq$0.6 Pa and room temperature). Silicone-like layers were deposited by a plasma enhanced chemical vapor deposition (PECVD) process from the silicon organic monomer hexamethyldisiloxane (HMDSO) at 20 W rf power, a pressure of 1.8 Pa and room temperature.

The introduction of the hydrogen-permeable materials like Pd or plasma-polymerized HMDSO (pp-HMDSO) underneath the anode catalyst layer is intended to allow an improved accessibility to catalyst sites which are not directly adjacent to a micropore. A scheme of the layered structure on the porous graphite electrode is shown in Fig. 2. Hydrogen entering from the bottom towards the catalyst can not only be reduced at the catalytic

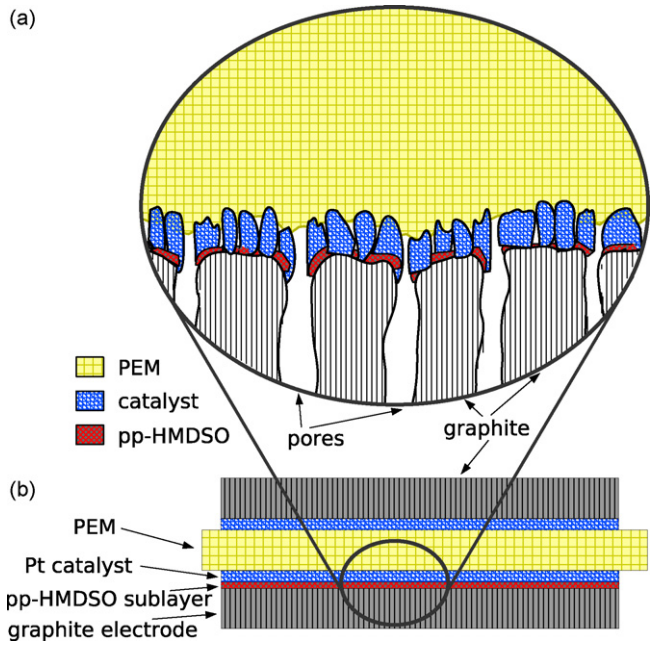

Fig. 2. Diagram of (b) a MEA consisting of porous electrodes with sputter-deposited catalyst layers, proton-conducting membrane (PEM), and a silicone-like pp-HMDSO sublayer on the anode side. The enlargement (a) shows the micro-porous graphite electrode with added hydrogen-permeable layer (pp-HMDSO) underneath the anode catalyst to promote a higher hydrogen distribution and accessibility of the catalyst.

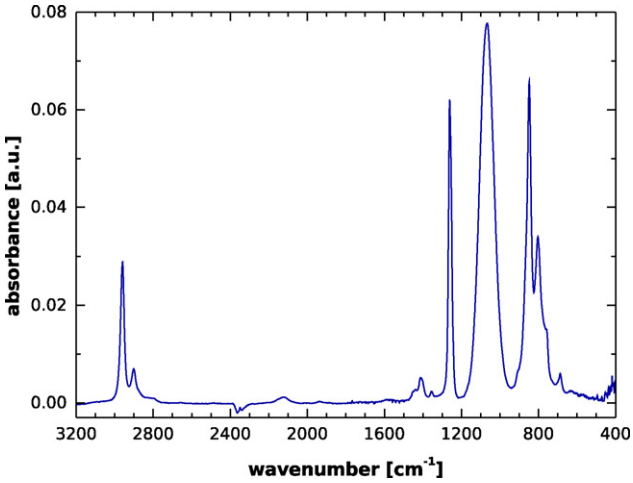

Fig. 3. FTIR spectrum of pp-HMDSO layer fabricated by plasma deposition from HMDSO with characteristic vibration modes of Si—O—Si between 1100 and 1000 cm^{-1}, Si—$(CH_3)_n$ at 1410 and 1260 cm^{-1}, Si—$(CH_3)_3$ end group near 850 cm^{-1}, and cyclic compound Si—$(CH_3)_2$ near 805 cm^{-1}.

sites directly at the pore but can move sideways through the pp-HMDSO (or Pd) to alternative catalytic sites that would otherwise be inactive. Data for the hydrogen permeability of the pp-HMDSO layer and silicone was shown elsewhere [34,35] and equally reported for Pd [36,37].

The pp-HMDSO layers were analyzed by taking Fourier transform infrared (FTIR) spectra (Spectrum GX, Perkin-Elmer). Sputtered catalyst thin layers were characterized by scanning electron microscopy (SEM) photographs (LEO 1530 Gemini, LEO Electron Microscopy) and energy dispersive X-ray (EDX) analysis (Link ISIS 300, Oxford Instruments) used to map the surface distribution of, e.g., the elements Pt, C, or F on the electrodes (with a fixed window size set to 7.53 μm × 5.65 μm and a repetition of 500 frames).

3. Results and discussion

Next to the aforementioned addition of thin layers of Pd before the deposition of the anode catalyst, silicone-like pp-HMDSO was analogously inserted to the anode side electrode prior to the deposition of the Pt catalyst.

A FTIR spectrum of a deposited pp-HMDSO thin film layer is depicted in Fig. 3. Its absorption bands can be assigned according to the literature [38]. The spectrum shows a strong Si–O–Si stretching vibration between 1090 and 1020 cm^{-1}. It overlaps with the Si–CH_2–Si vibration (1080–1040 cm^{-1}) which is accompanied by a much weaker peak at 1350 cm^{-1} due to the Si–CH_2–Si scissor vibration. The existance of this very weak absorption proves the additional polymerization via Si–CH_2–Si. In contrast to the Si–O–Si and Si –CH_2–Si bridges in the range 1090–1020 cm^{-1}, it can be clearly identified from this peak and is one of the polymerization mechanism of HMDSO [39]. Methyl groups attached to Si have a very sharp band at about 1260 cm^{-1} due to the symmetric deformation vibration of the CH_3 group. Their asymmetric deformation results in a weak band near 1410 cm^{-1}. At about 850 and 805 cm^{-1} the sharp band of Si–$(CH_3)_n$ end group ($n = 3$) and cyclic compounds ($n = 2$) vibration can be seen, respectively. The distinct peaks near 2960 and 2905 cm^{-1} correspond to CH stretching in CH_3 and CH_2, respectively. No O–H, C=O, and C=C is formed in the plasma polymerization process as modes in the ranges 3600–3200, 1850–1600, and 1580–1475 cm^{-1} are absent. These results proof that a silicone-like layer is successfully plasma-polymerized from HMDSO. Previous research exhibited that the permeability of hydrogen for this type of material is high [34], which should beneficially affect a homogeneous hydrogen fuel supply in fuel cells.

Fig. 4 depicts porous ELAT electrodes with a 0.054 mg cm^{-2} (25 nm) Pt layer on pp-HMDSO thin layers of 4, 20, and 55 nm thickness (measured on a non-porous reference sample). In the SEM image for the 4 nm pp-HMDSO layer, only the Pt layer on the micro-porous graphite substrate can be identified. With increased pp-HMDSO layer thickness (Fig. 4b and c) and equal Pt loading, the pp-HMDSO layer spreads out across the porous ELAT electrode and obturates first micropores. The non-conductive pp-HMDSO layer already generates charging effects due to the scanning electron beam at these increased layer thicknesses, i.e., they are likely to negatively influence the electrode's performance in fuel cells because of increased ohmic resistances. This was proven by measuring the resistance with the current interrupt method [40]. The MEA resistance increases according to the five bars on the left in Fig. 5 as the pp-HMDSO layer thickness rises from 0 to 110 nm.

SEM images of 0.005 and 0.054 mg cm^{-2} Pt on porous electrodes are shown in Fig. 6 along with 0.054 mg cm^{-2} Pt on a 1 nm thin sublayer of Cr on the left and their EDX mapping images

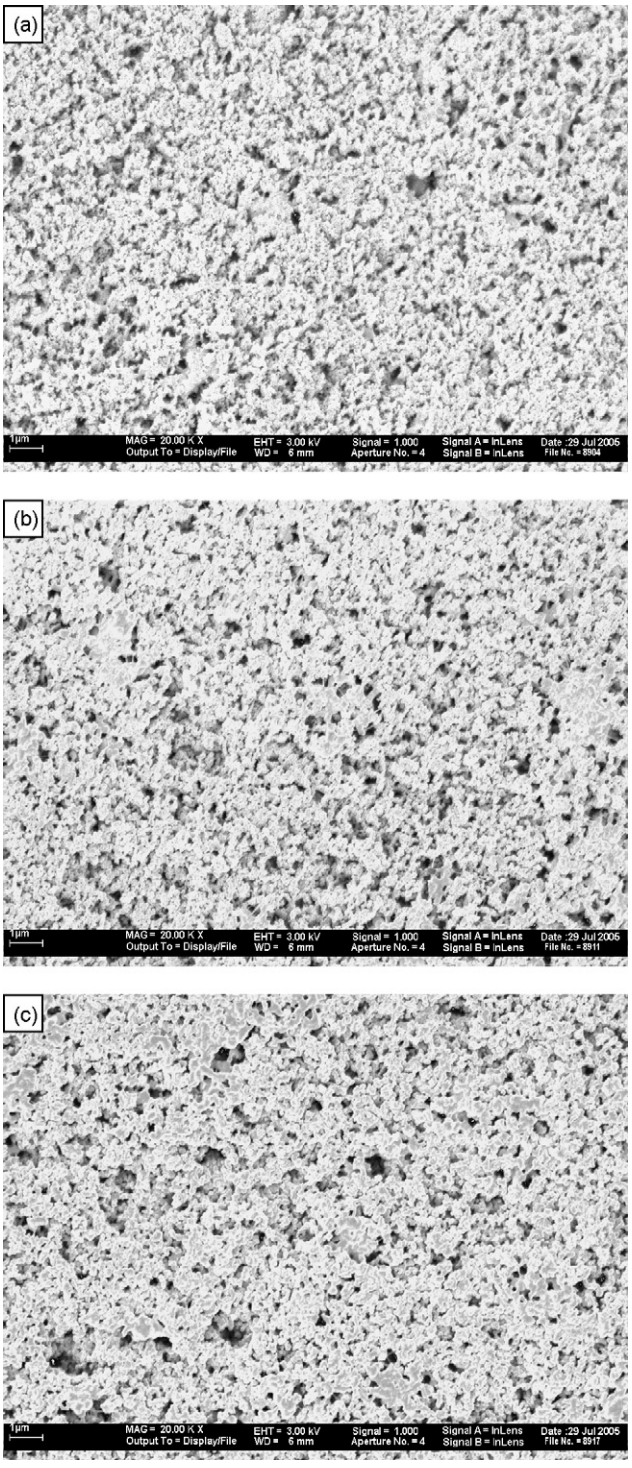

Fig. 4. A thin film of 25 nm Pt on silicone-like pp-HMDSO sublayers of (a) 4 nm, (b) 20 nm, and (c) 55 nm on uncatalyzed ELAT electrodes.

of the element Pt of the same detail on the right. By comparing the images of 0.054 mg cm^{-2} Pt on the Cr sublayer with that without this sublayer, a distinct and more continuous distribution of the Pt catalyst particles is apparent. When accumulating the number of pixels according to their intensity (white representing the mapped element Pt) in Fig. 6(5) and (6) their amount is increased when Pt is deposited on the Cr sublayer (see Fig. 7).

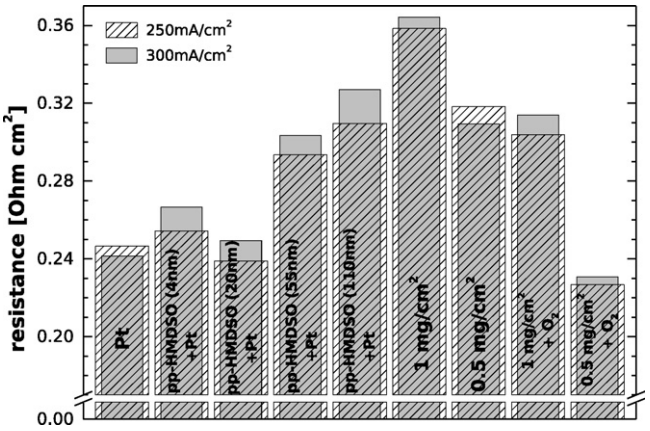

Fig. 5. Ohmic MEA resistance as determined by the current interrupt technique from the immediate voltage rise recorded with an oscilloscope after interrupting the current (250 and 300 mA cm^{-2}) for samples with 0.054 mg cm^{-2} sputter-deposited Pt and 0, 4, 20, 55, 110 nm pp-HMDSO layer thickness added. In addition resistances are shown for commercial catalyzed ELAT electrodes loaded with 1 and 0.5 mg cm^{-2} Pt with and without a 3 min O_2 plasma treatment.

Assuming that the topological differences of each investigated sample level out over all tested samples, this indicates that the Pt on the Cr sublayer is more evenly distributed across the electrode as compared to the same Pt loading sputter-deposited directly on the electrode.

This is in accordance with the previously presented results [33], where two thin sublayers of Cr were introduced into the Pt catalyst layer, i.e., Cr was not deposited as a first layer or seeding layer. The process of the simple integration of a single Cr sublayer presented here, however, has the same morphological effect.

The graphs in Figs. 8 and 9 show the characteristic curves for the fuel cells with the differently prepared catalysts loaded with 0.054 mg cm^{-2} (25 nm) of sputter-deposited Pt. Other curves in the graphs represent measurements for fuel cells prepared with electrodes loaded with 0.005 mg cm^{-2} (2.5 nm) Pt and cells prepared from catalyzed ELAT electrodes commercially loaded with 0.5 mg cm^{-2} Pt. From comparing the results of the electrodes with 0.054 mg cm^{-2} Pt loading in the graph it can be seen that the insertion of Pd (20 nm) or pp-HMDSO (4 nm) on the anode side as well as the introduction of thin layers of Cr (1 nm) on both electrodes improve the performance. The addition of the Pd and pp-HMDSO layer underneath the anode catalyst improves the peak power density by about 8 and 18%, respectively. The thin layer of Cr under the Pt catalyst loading of 0.054 mg cm^{-2} increases the maximum power density from 210 mW cm^{-2} for the fuel cell with conventionally sputter-deposited Pt to 256 mW cm^{-2} for the cell with the Pt catalyst sputtered on a 1 nm thin Cr layer. This is an increase of the peak power density by slightly more than 23%.

The very simple additional process of introducing a Cr seed layer proves to be very effective to achieve a more dispersed and by this more efficient catalyst layer at low Pt loading. In comparison with the previous results, where two thin layers of Cr had been inserted into the Pt catalyst, the performance is even more improved since the Cr seeds offer a more dispersed low energetic starting basis for the steady growth of Pt catalyst

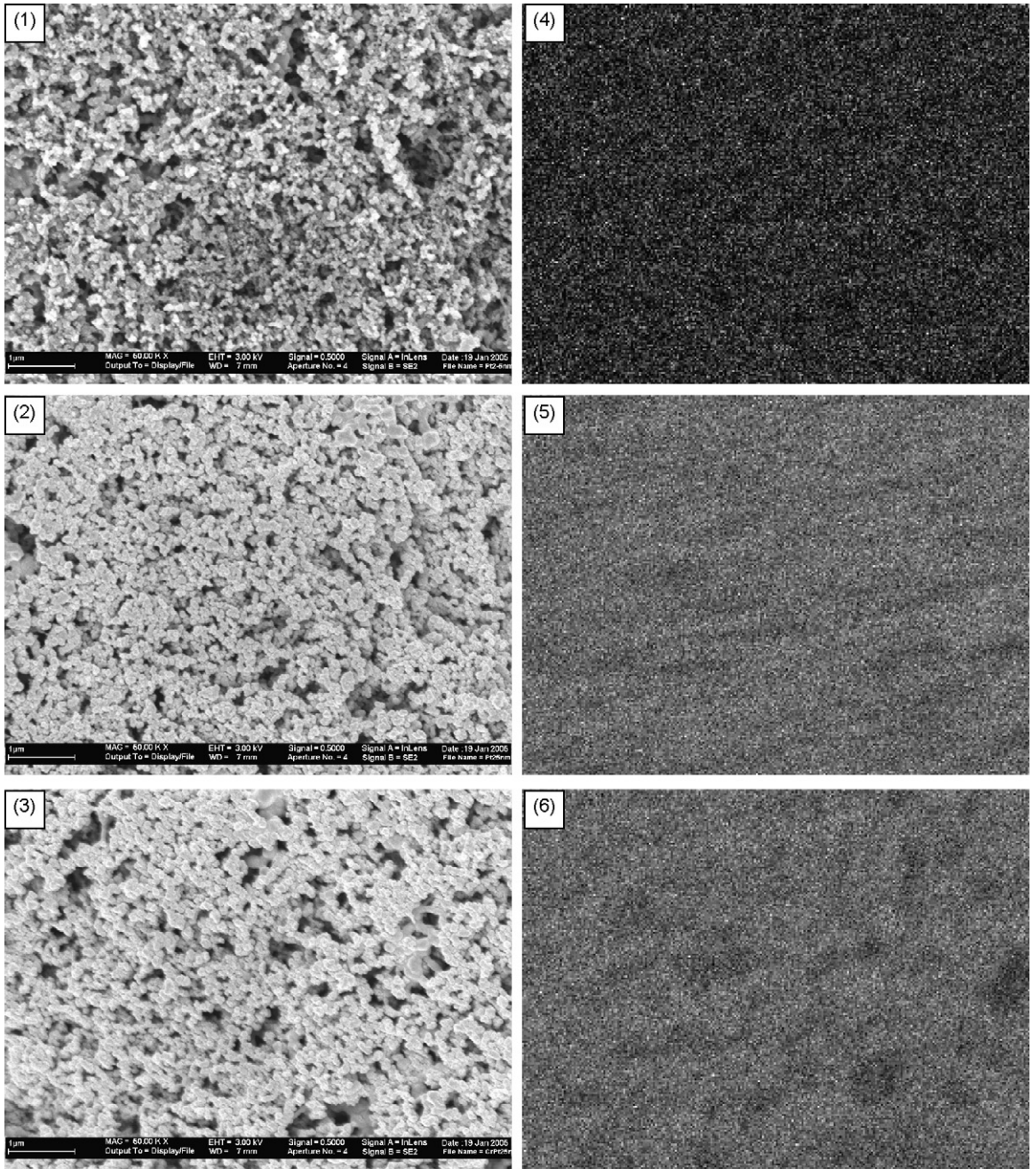

Fig. 6. SEM images of uncatalyzed ELAT electrodes with (1) 2.5 nm Pt, (2) 25 nm Pt, and (3) 25 nm Pt on a 1 nm Cr seeding layer. EDX mapping for Pt of the electrodes is shown on the right hand side of each SEM image, i.e., for (4) 2.5 nm Pt, (5) 25 nm Pt, and (6) 25 nm Pt on Cr.

clusters than does a solely deposited Pt catalyst base with added Cr intermediate layers.

The graphs show also the characteristic curves for ELAT electrodes loaded with just 0.005 mg cm^{-2} Pt. For miniaturized fuel cells it was shown that the loading on the anode side can be reduced from 0.054 mg cm^{-2} to this ultra-low Pt loading without decreasing the performance [41] due to the high electrocatalytic activity of Pt towards hydrogen oxidation.

The Pt mass specific power density of the MEAs with electrode loadings of 0.054 mg cm^{-2} Pt on a thin film of Cr is 0.5 g kW^{-1} at 0.6 V and ambient conditions, whereas it is 0.6 g kW^{-1} without the Cr thin film. The MEA's Pt mass specific power density is 0.15 g kW^{-1} when reducing both electrode loadings to 0.005 mg cm^{-2} Pt.

The graphs in Figs. 10 and 11 show the characteristic curves for fuel cells prepared with commercial catalyzed ELAT electrodes with 0.5 and 1 mg cm^{-2} Pt loading. Their performance improves after treating the surface of the catalyzed ELAT electrodes in an O_2 plasma. The peak power density for the fuel cells with a catalyzed ELAT electrode loading of 1 mg cm^{-2} Pt, for example, improves from 235 mW cm^{-2} to 282 mW cm^{-2} after the oxygen plasma treatment. This is an improvement of

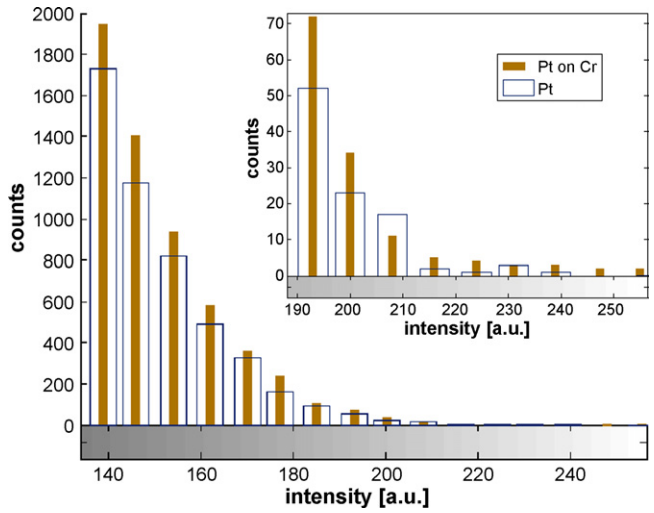

Fig. 7. Counts of EDX mapped pixels representing the element Pt vs. their intensity. White or intensity of 256 represents pure Pt spots. The inset shows an enlargement of the high intensity region.

20%. For the commercial electrode with 0.5 mg cm^{-2} Pt the enhancement was of approximately the same order. From EDX mapping investigations to study the close to surface distribution of the elements C, F, and Pt it can be concluded that in the plasma carbon-containing species are burned from the surface and expose or uncover more Pt catalyst on the surface. This increases the Pt catalyst density on the surface of the electrode at the interface with the PEM. This effect is similar to the boost in performance achieved by the sputter deposition of Pt on top of commercially available Pt gas diffusion electrodes already loaded with regular carbon-supported Pt catalyst [42]. Fig. 12 shows the counts representing carbon concentration for the normal catalyzed ELAT electrode with 1 mg cm^{-2} Pt and the same electrode exposed to a 3 min oxygen plasma. The number of

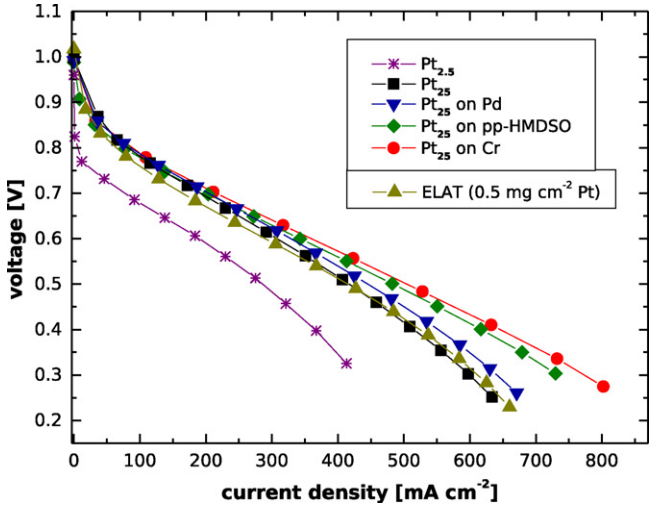

Fig. 8. Polarization curves for fuel cells with sputter-deposited 0.054 mg cm^{-2} (25 nm) Pt catalyst (Pt$_{25}$) and different added sublayers. For reference the results for fuel cells prepared with 0.005 mg cm^{-2} (2.5 nm) Pt (Pt$_{2.5}$) and commercial catalyzed ELAT electrodes with 0.5 mg cm^{-2} Pt loading are shown.

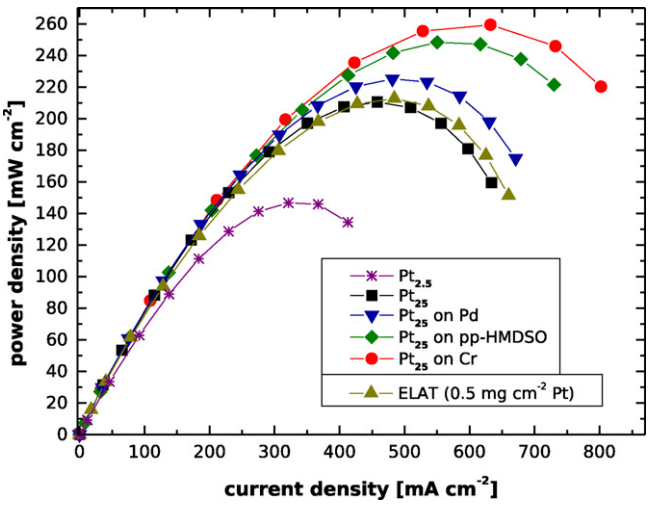

Fig. 9. Power density vs. current density for fuel cells with 0.054 mg cm^{-2} (25 nm) sputter-deposited Pt catalyst (Pt$_{25}$) and different added sublayers along with the results for fuel cells prepared with 0.005 mg cm^{-2} (2.5 nm) Pt (Pt$_{2.5}$) and a catalyzed ELAT electrodes loaded with 0.5 mg cm^{-2} Pt are shown.

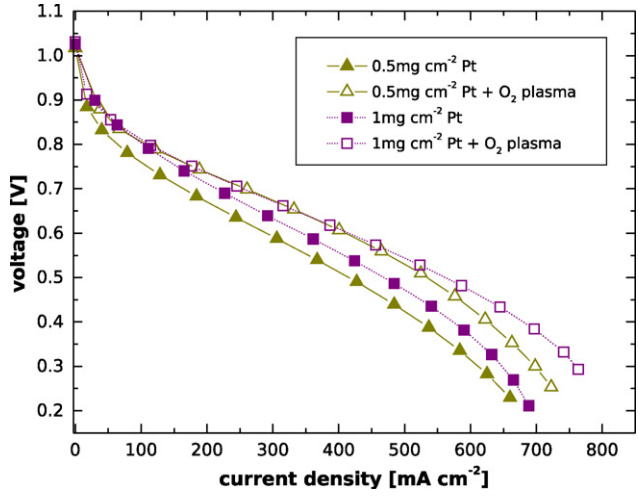

Fig. 10. Polarization curves of normal and O_2 plasma treated commercial catalyzed ELAT electrodes (0.5 and 1 mg cm^{-2} Pt).

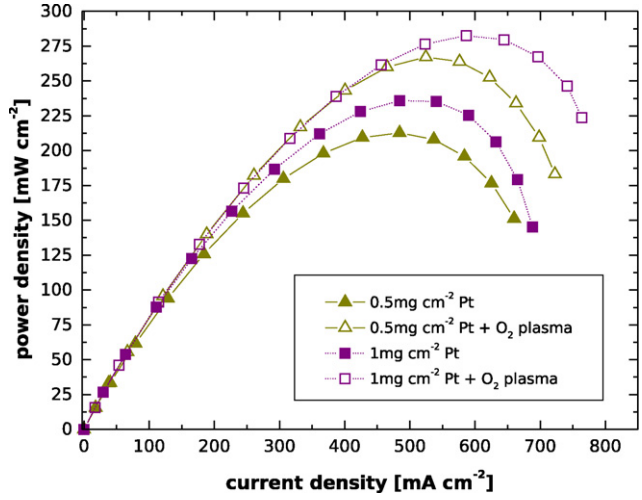

Fig. 11. Power density vs. current density of normal and O_2 plasma treated commercial catalyzed ELAT electrodes (0.5 and 1 mg cm^{-2} Pt).

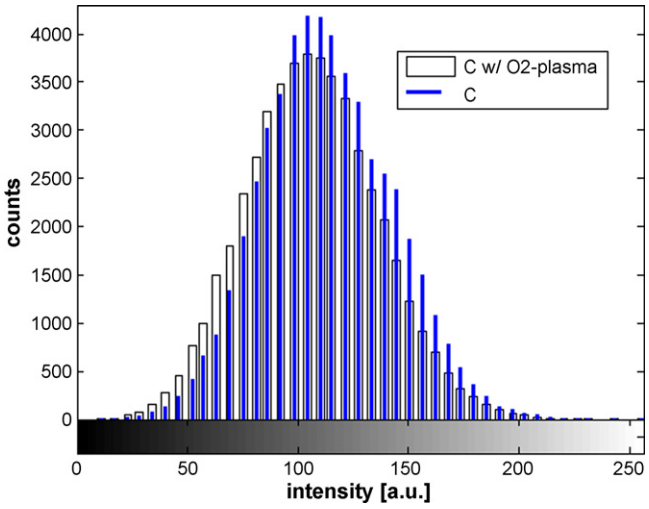

Fig. 12. Counts of EDX mapped pixels representing the element C vs. their intensity. White or intensity of 256 represents pure C spots.

counts at high intensities is shifted to lower intensities. This stands for a decrease of spots containing carbon only or mostly carbon towards a mix of carbon with other species (namely Pt) as the emphasis of lower intensities increases. The reverse effect is observed for the platinum distribution. The shift coincides with a lower MEA resistance after the 3 min O_2 plasma treatment as can be seen from Fig. 5.

4. Conclusion

Catalyst layers with low Pt loadings applied by sputter deposition on standard gas diffusion layer substrates can be made more effective by adding additional sublayers. The insertion of the hydrogen-permeable materials Pd or silicone-like pp-HMDSO sublayers underneath the anode catalyst thin film improves the performance of the fuel cells of up to 18%. It is assumed that higher access of hydrogen is allowed to anode catalyst sites which not directly border micropores. The addition of a thin film of Cr on both electrodes before the sputter deposition of the Pt catalyst has a similar effect due to a change in morphology. The effectiveness of the Pt catalyst is improved by its more evenly distributed growth on the Cr seeds. With a Pt loading per electrode of 0.054 mg cm^{-2} on a 1 nm Cr thin film the platinum mass specific power density for MEAs at 0.6 V and ambient conditions could be reduced to 0.5 g kW^{-1}. A reduction of 20% compared to the samples prepared without the Cr thin films. Future durability experiments will need to prove the long time stability of these catalysts.

The reference MEAs prepared from commercial catalyzed ELAT electrodes loaded with 0.5 mg cm^{-2} Pt could not outperform the cells prepared with low-loaded (0.054 mg cm^{-2}) sputter-deposited Pt catalyst. Their Pt mass specific power density is clearly >1 g kW^{-1}. However, their performance could be improved by exposing them to an O_2 plasma which removes surface located carbon and PTFE elements from the electrode surface and by this increases the available Pt catalyst sites allocated to the electrode–PEM boundary.

Acknowledgment

The financial support of this work by the German Federal Ministry of Economics and Technology (Bundesministerium für Wirtschaft und Technologie, BMWi) is gratefully acknowledged.

References

[1] D.J. Berger, Science 286 (1999) 49.
[2] B. Wang, J. Power Sources 152 (2005) 1–15.
[3] R. Benítez, A.M. Chaparro, L. Daza, J. Power Sources 151 (2005) 2–10.
[4] M.J. Escudero, E. Hontañón, S. Schwartz, M. Boutonnet, L. Daza, J. Power Sources 106 (2002) 206–214.
[5] S. Gamburzev, A.J. Appleby, J. Power Sources 107 (2002) 5–12.
[6] L. Xiong, A. Manthiram, Electrochim. Acta 50 (2005) 3200–3204.
[7] S.Y. Cha, W.M. Lee, J. Electrochem. Soc. 146 (1999) 4055–4060.
[8] A.T. Haug, R.E. White, J.W. Weidner, W. Huang, S. Shi, T. Stoner, N. Rana, J. Electrochem. Soc. 149 (2002) A280–A287.
[9] T. Nakakubo, M. Shibata, K. Yasuda, J. Electrochem. Soc. 152 (2005) A2316–A2322.
[10] K. Makino, K. Furukawa, K. Okajima, M. Sudoh, Electrochim. Acta 51 (2005) 961–965.
[11] S.R. Brankovic, J.X. Wang, R.R. Adžić, Electrochem, Solid-State Lett. 4 (2001) A217–A220.
[12] K. Sasaki, Y. Moa, J.X. Wang, M. Balasubramanian, F. Uribe, J. McBreen, R.R. Adžić, Electrochim. Acta 48 (2003) 3841–3849.
[13] K. Sasaki, J.X. Wang, M. Balasubramanian, J. McBreen, F. Uribe, R.R. Adžić, Electrochim. Acta 49 (2004) 3873–3877.
[14] S.R. Brankovic, J.X. Wang, Y. Zhu, R. Sabatini, J. McBreen, R.R. Adžić, J. Electroanal. Chem. 524 (2002) 231–241.
[15] A.F. Gullá, M.S. Saha, R.J. Allen, S. Mukerjee, Electrochem. Solid-State Lett. 8 (2005) A504–A508.
[16] S. Mukerjee, S. Srinivasan, J. Electroanal. Chem. 357 (1993) 201–224.
[17] S.-A. Lee, K.-W. Park, J.-H. Choi, B.-K. Kwon, Y.-E. Sung, J. Electrochem. Soc. 149 (2002) A1299–A1304.
[18] T. Toda, H. Igarashi, M. Watanabe, J. Electroanal. Chem. 460 (1999) 258–262.
[19] F.A. Uribe, T.A. Zawodzinski Jr., Electrochim. Acta 47 (2002) 3799–3806.
[20] H. Uchida, H. Ozuka, M. Watanabe, Electrochim. Acta 47 (2002) 3629–3636.
[21] G. Samjeské, H. Wang, T. Löffler, H. Baltruschat, Electrochim. Acta 47 (2002) 3681–3692.
[22] E. Antolini, J. Appl. Electrochem. 34 (2004) 563–576.
[23] V. Jalan, E.J. Taylor, J. Electrochem. Soc. 130 (1983) 2299–2302.
[24] T. Toda, H. Igarashi, M. Watanabe, J. Electrochem. Soc. 145 (1998) 4185–4188.
[25] S. Mukerjee, S. Srinivasan, M.P. Soriaga, J. McBreen, J. Phys. Chem. 99 (1995) 4577–4589.
[26] C.A. Bessel, K. Laubernds, N.M. Rodriguez, R.T.K. Baker, J. Phys. Chem. B 105 (2001) 1115–1118.
[27] K.-W. Park, Y.-E. Sung, S. Han, Y. Yun, T. Hyeon, J. Phys. Chem. B 108 (2004) 939–944.
[28] E.S. Steigerwalt, G.A. Deluga, D.E. Cliffel, C.M. Lukehart, J. Phys. Chem. B 105 (2001) 8097–8101.
[29] E.S. Steigerwalt, G.A. Deluga, C.M. Lukehart, J. Phys. Chem. B 106 (2002) 760–766.
[30] M.M. Waje, X. Wang, W. Li, Y. Yan, Nanotechnology 16 (2005) S395–S400.
[31] X. Wang, M. Waje, Y. Yan, Electrochem. Solid-State Lett. 8 (2005) A42–A44.
[32] K. Lee, J. Zhang, H. Wang, D.P. Wilkinson, J. Appl. Electrochem. 36 (2006) 507–522.
[33] D. Gruber, N. Ponath, J. Müller, F. Lindstaedt, J. Power Sources 150 (2005) 67–72.
[34] S. Nehlsen, T. Hunte, J. Müller, J. Membr. Sci. 106 (1995) 1–7.

[35] W.L. Robb, Ann. NY Acad. Sci. 146 (1968) 119–137.
[36] T. Graham, Phil. Trans. R. Soc. Lond. 156 (1866) 399–439.
[37] A.G. Knapton, Plat. Met. Rev. 21 (1977) 44–50.
[38] G. Socrates, Infrared Characteristic Group Frequencies, 2nd ed., John Wiley & Sons, Chichester, 1994.
[39] C. Rau, W. Kulisch, Thin Solid Films 249 (1994) 28–37.
[40] J. Larminie, A. Dicks, Fuel Cell Systems Explained, John Wiley & Sons, Chichester, 2002, pp. 56–59.
[41] D. Gruber, N. Ponath, J. Müller, Electrochim. Acta 51 (2005) 701–705.
[42] S. Mukerjee, S. Srinivasan, A.J. Appleby, Electrochim. Acta 38 (1993) 1661–1669.